UNIVERSITA' DI NAPOLI FEDERICO II

DOTTORATO DI RICERCA IN
BIOCHIMICA E BIOLOGIA CELLULARE E MOLECOLARE
XXVI CICLO

BIOSILICA NANOVECTOR FROM DIATOMITE FOR siRNA TRANSPORT IN CANCER CELL
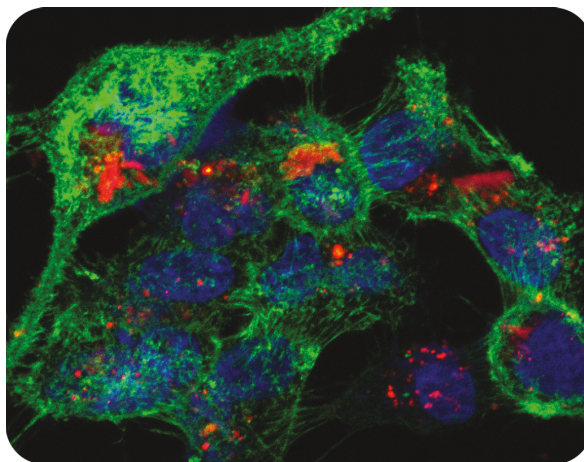
Candidate
Nunzia Migliaccio

Tutor
Dott.ssa Annalisa Lamberti

Coordinator
Prof. Paolo Arcari

Academic Year 2013/2014

Riassunto

La diatomite è un biomateriale poroso naturale di origine sedimentaria, formata da frammenti di scheletri silicei di diatomee, chiamati "frustoli". Grazie alla grande disponibilità in molte aree del mondo, alla stabilità chimica e alla non tossicità, questo materiale fossile ha trovato largo impiego in molte applicazioni industriali, come la produzione di cibo, la purificazione dell'acqua attraverso l'estrazione di agenti tossici, la produzione di cosmetici e di prodotti farmaceutici. Tuttavia, le diatomiti non sono state ancora utilizzate in applicazioni biomediche.

Nel presente studio, è stata esplorata la possibilità di utilizzare le diatomiti per la realizzazione di nanovettori per il *delivery* di molecole antitumorali.

Per rimuovere le impurezze inorganiche e organiche dalle diatomiti e renderle un materiale sicuro per applicazioni mediche è necessaria una procedura di purificazione, basata sul trattamento con soluzioni calde di acidi forti. La polvere micrometrica è stata ridotta in nanoparticelle attraverso frantumazione meccanica, sonicazione e filtraggio.

La morfologia e la composizione delle diatomiti sono state studiate mediante microscopia elettronica a scansione dotata di spettroscopia a raggi X a dispersione di energia, fotoluminescenza e misure di DLS. Esperimenti in vitro hanno mostrato una tossicità molto bassa dopo esposizione di cellule a concentrazioni di diatomiti fino a 300 μg/ml per 72 h.

Le nanoparticelle sono state successivamente funzionalizzate con un derivato del silano (APTES) e marcate con tetrametilrodamina isotiocianato. Diverse concentrazioni di diatomiti marcate sono state incubate con le cellule tumorali e sono state osservate al microscopio confocale che ha mostrato un'effettiva internalizzazione cellulare e una distribuzione omogenea delle nanoparticelle sia nel citoplasma sia nel nucleo, suggerendo così la possibilità di utilizzare tali nanovettori per il *delivery* di farmaci.

Successivamente, attraverso l'utilizzo di un *linker*, è stato caricato un siRNA fluorescente e l'analisi attraverso microscopia confocale, in

questo caso, ha mostrato una localizzazione esclusivamente citoplasmatica del vettore. Inoltre, utilizzando un siRNA specifico, è stato ottenuto silenziamento genico.

I nostri studi suggeriscono che le diatomiti rappresentano un promettente biomateriale per lo sviluppo di nanovettori non tossici per il trasporto di siRNA in cellule tumorali.

Summary

Diatomite is a natural porous biomaterial of sedimentary origin, formed by fragments of diatom siliceous skeletons, called "frustules". Due to large availability in many areas of the world, chemical stability, and non-toxicity, these fossil structures have been widespread used in a lot of industrial applications, such as food production, water extracting agent, production of cosmetics and pharmaceutics. However, diatomite is surprisingly still rarely used in biomedical applications.

In this study, the properties of diatomite nanoparticles as potential system for the delivery of anticancer molecules in cancer cells were exploited.

A purification procedure, based on thermal treatments in strong acid solutions, was used to remove inorganic and organic impurities from diatomite and to make them a safe material for medical applications. The micrometric diatomite powder was reduced in nanoparticles by mechanical crushing, sonication, and filtering.

Morphology and composition of diatomite were investigated by scanning electron microscopy equipped by energy dispersive X-ray spectroscopy, photoluminescence and dynamic light scattering measurements. In-vitro experiments show a very low toxicity on exposure of the cells to diatomite nanoparticle concentration up to 300 µg/ml for 72 h.

Diatomite nanoparticles were functionalized by 3-aminopropyltriethoxysilane and labeled by tetramethylrhodamine isothiocyanate. Different concentrations of chemically modified nanoparticles were incubated with cancer cells and confocal microscopy was performed. Imaging analysis showed an efficient cellular uptake and homogeneous distribution of nanoparticles in cytoplasm and nucleus, thus suggesting their potentiality as nanocarriers for drug delivery.

Subsequently, siRNA bioconjugation were performed and confocal microscopy imaging on cancer cells incubated with siRNA-conjugated nanoparticles demonstrated a cytoplasmatic localization of

vectors. Gene silencing by delivered siRNA was also demonstrated. Our studies endorse diatomite nanoparticles as non-toxic nanocarriers for siRNA transport in cancer cells. siRNA-diatomite nanoconjugate may be well suited for delivery of therapeutic to cancer cells.

Index

List of Figure and Tables

List of Abbreviations

NPs: Nanoparticles;

siRNA: small interfering Ribonucleic Acid;

MTT: 3-(4,5- dimethythiazol-2-yl)-2,5-diphenyl tetrazolium bromide;

APTES: (3-aminopropyl)triethoxysilane;

TCEP: Tris(2carboxyethyl)phosphine hydrochloride;

PBS: Phosphate buffered saline;

Sulfo-GMBS: N-(γ-Maleimidobutyryloxy) sulfosuccinimide ester;

SEM: Scanning Electron Microscopy;

DLS: Dynamic Light Scattering;

PL: Photoluminscence;

EDS: Energy Dispersive X-ray Spectroscopy;

DNPs: Diatomite Nanoparticles;

TRITC: tetramethylrhodamine isothiocyanate;

DMSO: dimethyl sulfoxide;

FBS: Fetal Bovine Serum;

RPMI: Roswell Park Memorial Institute medium;

FTIR: Fourier Transformed Infrared**;**

EMSA: Elettrophoretic Mobility Shift Assay;

TAE: Tris Acetate EDTA;

HP-RNase: Human Pancreatic Ribonuclease;

1. Introduction

1.1 Drug delivery

The drug delivery is a research field that has captured the interest and curiosity of researchers because delivering a medicine to its site of therapeutic action is one of the main limitations of pharmaceutical and biotechnology industries [1] The drug delivery can be defined as a releasing process of a bioactive agent at a specific rate and at a specific site. The targeted drug delivery can be useful to exploit thousands of new therapeutics that are limited by a safe and effective drug-delivery system [1,2]. The discovery of new drugs classes is crucial to set up specific drug-delivery methods to activate these new advances into clinical effectiveness. The conventional drugs are limited by their poor solubility, non specific delivery, high toxicity, high dosage, in vivo degradation and short circulating half-lives, but at present, the field of drug delivery is developing rapidly to reduce the drugs' ever-increasing problems [1]. The drug delivery field has also attracted the attention of the pharmaceutical industry because it offers new tools to develop current drug markets. Targeted drug-delivery systems can transport drugs more effectively then the conventional system and it can extend the provide product differentiation, product life cycle, and reduce patient healthcare costs [3]. In addition, these systems would improve the pharmacokinetics and the short half-lives of degradable peptides and proteins in vivo [4,5]. Therefore, one of the most important areas of drug research is the development of techniques that could selectively deliver drugs to the pathological sites [6]. NPs can be correctly envisioned as the future of drug-delivery technology as they have the potential to become useful therapeutic and diagnostic tools in the near future [7].

1.2 Nanotechnology as a solution for drug delivery

Nanotechnology is the creation and handling of materials, devices and systems through the control of matter on the nanometer-length scale.

Due to the small size and dimensional similarities to biomolecules, nanomaterials exhibit a far greater intracellular uptake as compared with micro sized particles, making them excellent candidates for targeted drug delivery [8]. More importantly, nanomaterials also offer attractive possibilities to circumvent the vascular barriers and biological defense systems of the body. For instance, micro sized particles are easily taken up by the macrophages widely distributed throughout the body and this leads to rapid clearance of the microparticles from the bloodstream by the reticulo endothelial defence mechanism [9,10]. Considering that extremely tiny capillaries, of about 2.3 micrometers in diameter, have been observed [11], well designed nanomaterials of controlled size range (sub-200 nm) can increase the opportunities to deliver drug payloads precisely to the diseases.

Furthermore, nanomaterials can carry a large number of imaging and/or therapeutic agents owing to their enormous surface area relative to their total volume. For example, a polymeric nanoparticle having an average diameter of 70 nm is able to contain approximately 2,000 drug molecules [12], while a polymer-drug conjugate carries only nine drug molecules per molecule [13]. In addition they offer a possibility of surface modification with multiple targeting moieties (such as small molecules, peptides, or antibodies) for effective disease targeting. Recent researches have proven that the multiple attachment of a targeting ligand significantly enhances the intracellular uptake of the ligand-functionalized nanovehicles in the target cancer cells via the multivalent binding to the cell-surface receptors [14,15]. Hence a nanocarrier system possessing a number of targeting ligands can be effectively exploited for targeting to the tumor tissues with a specific uptake.

Nanotechnology focuses on formulating therapeutic agents in biocompatible nanocarriers, including polymeric NPs, ceramic NPs, magnetic NPs, polymeric micelles and dendrimers.

A successful nanocarrier should ideally meet the following

requirements: (1) formulation with biocompatible and/or biodegradable materials, (2) high drug loading capacity, (3) site-specific delivery mechanism to avoid normal cells and tissues, (4) zero or negligible premature drug release, and (5) controlled release mechanism to provide an effective dose to the target site [16]. A natural material that possesses those features is represented by diatomite.

1.3 Diatomite

Diatomaceous earth, also known as diatomite, is a fossil material of sedimentary origin, formed over centuries by siliceous skeleton (called "frustule") of aquatic unicellular microalgae, the diatoms, deposited on bottom of lakes or present in marine environments. Diatomite morphology can be very complex due to the presence of diatom frustules with different sizes (ranging from 2 μm to 2 mm) and shapes. The structure is highly porous and characterized by a large specific surface area up to 200 m^2/g [17]. The main constituent of diatomite is amorphous silica (70% - 90%), although it can contain impurities such as organic components and metallic oxides (MgO, Al_2O_3, Fe_2O_3) coming from environment [17,18]. Different strategies, including calcination processes and hot acid treatments, have been developed to remove impurities from frustules [19,20]. Due to large availability in many areas of the world, chemical stability, and non-toxicity, this fossil material has been widespread used in lot of industrial applications, such as food production, water extracting agent, production of cosmetics and pharmaceutics [21-24].

Recently, diatom frustules have been exploited as an innovative platform in several biotechnological applications [25,26]. In fact, the silica surface of diatoms, covered by reactive silanol (Si-OH) groups, can be modified with functional reactive groups (-NH_2, -COOH, -SH, -CHO) for the immobilization of biomolecular probes (DNA, antibodies, enzymes) [27]. Moreover, the porous structure allows the binding of a large amount of bioprobe molecules with respect to a flat

surface, thus increasing sensitivity of biosensing. In recent works, we reported the chemical modification of marine diatom frustules with antibody as highly selective bioprobe. The antibody–antigen molecular recognition was investigated by means of photoluminescence and fluorescence microscopy [28,29].

Although diatomite, differently from diatom frustules, is a cheaper material produced in tons by mining industry, it is surprisingly still scarcely used in biomedical applications. Recent pioneering papers demonstrated the use of diatomite as microcapsules for oral drug delivery [30,31].
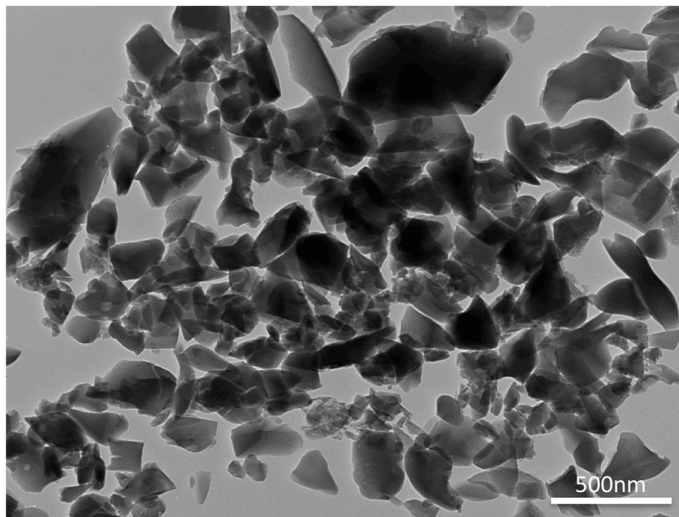
Figure 1 TEM image of diatomite nanoparticles

1.4 Scientific hypothesis and aim of the work

In this work, porous diatomite nanocarriers, with an average diameter less than 450 nm, were bioconjugated with small interfering ribonucleic acid (siRNA) in order to test their drug delivery capability. As a matter of fact, siRNA is a powerful approach for silencing genes associated with a variety of pathologic conditions but

its systemic delivery is inefficient due to the difficulty to penetrate the cell membrane [32,33]; its conjugation to nanovectors (including liposomes, gold and magnetic nanoparticles, quantum dots) is one of the possible strategies developed to overcome this challenging problem [34,35]. In particular, we have investigated diatomite nanoparticles cytotoxicity and examined their ability to transport siRNA inside cancer cells and to silence gene expression. The results, compared with those reported in literature on standard systems [36,37], encourage the use of diatomite nanoparticles as drug carriers.

2. Materials and Methods

2.1 Materials
Calcined diatomite was obtained by DEREF Spa (Italy); 3-(4,5-dimethythiazol-2-yl)-2,5-diphenyl tetrazolium bromide (MTT), (3-aminopropyl)triethoxysilane (APTES), Tris(2carboxyethyl)phosphine hydrochloride (TCEP), tetramethylrhodamine isothiocyanate (TRITC), dimethyl sulfoxide (DMSO) and H_2SO_4 were purchased from Sigma-Aldrich (MO, USA). Phosphate buffered saline (PBS) was purchased from GIBCO (CA, USA). N-(γ-Maleimidobutyryloxy) sulfosuc-cinimide ester (Sulfo-GMBS), on target plus smart pool human GAPDH (siRNA GAPDH), on target plus control pool non-targeting pool (siRNA scramble, SCR) and siGLO RISC-Free control siRNA (siGLO RNAi), chemically modified to impair processing and uptake by RISC, were from Thermo Scientific (MMedical, Milan, Italy). Synthesis of poly D-Arg peptide (sequence RRRRRRRC) and non-polar homopeptide was performed by Proteogenix (FR). HCl was purchased from Romil (UK). Absolute ethanol, Tris-(hydroxymethyl)aminomethane, NaCl and H_2O_2 were purchased from Carlo Erba (IT). Rabbit anti-GAPDH polyclonal antibody was purchased from Cell Signaling Technology Inc. (MA, USA). Rabbit anti-β-tubulin polyclonal antibody and goat anti-rabbit immunoglobulin conjugated to horseradish peroxidase were from Santa Cruz Biotechnology (CA, USA).

2.2 Diatomite purification treatment
5 g of diatomite powder was dissolved in 250 ml of absolute ethanol and sonicated for 5 h in order to break up macroscopic aggregates. The dispersion was filtered through a nylon net filter with pore size of 40 μm (Millipore) and then filtered with pore size of 0.45 μm (Millipore, Billerica, MA, USA). Dispersion of diatomite nano-particles was centrifuged at 15,000 ×g for 30 min, and the supernatant was removed.

Diatomite nanopowder was purified to remove organic and inorganic contaminants [17,19]. To this aim, diatomite dispersion was centrifuged and the pellet was suspended in piranha solution (2 M H_2SO_4, 10% H_2O_2) for 30 min at 80 °C. Dispersion was then centrifuged for 30 min at 15,000 ×g and supernatant was removed. Diatomite was washed twice with deionized water. Subsequently, 5.0 M HCl solution was added to diatomite and incubated overnight at 80 °C. After HCl incubation, diatomite dispersion was centrifuged for 30 min and supernatant was removed. Pellet was washed twice with deionized water that removed excess of HCl.

2.3 Characterization of nanoparticles size

Scanning electron microscopy (SEM) equipped with energy dispersive X-ray spectroscopy (EDS) (Fei, Quanta 200 FEG) was used to investigate nanoparticles morphology. Briefly, for SEM characterization diatomite samples were deposited on crystalline silicon substrates mounted on a double-faced conductive adhesive tape. Images were acquired at 5-kV accelerating voltage and 30-µm wide aperture.

The size and zeta-potential measurements of purified diatomite nanoparticles dispersed in water (pH = 7) were performed by dynamic light scattering (DLS) using a Zetasizer Nano ZS (Malvern Instruments, Malvern, UK) equipped with a He-Ne laser (633 nm, fixed scattering angle of 173°, 25°C).

2.4 Steady-state photoluminescence

Steady-state photoluminescence (PL) spectra were excited by a continuous wave He–Cd laser at 325 nm (KIMMON Laser System). PL was collected at normal incidence to the surface of samples through a fiber, dispersed in a spectrometer (Princeton Instruments, SpectraPro 300i), and detected using a Peltier cooled charge coupled device (CCD) camera (PIXIS 100F). A long pass filter with a nominal

cut-on wavelength of 365 nm was used to remove the laser line at monochromator inlet.

2.5 Cell culture

The human lung epidermoid carcinoma cell line (H1355) was obtained from the American Type Tissue Collection (Rockville, MD, USA). The cell line were grown in RPMI 1640 (GIBCO) medium supplemented with 10% heat inactivated FBS (GIBCO), 100 U/ml penicillin, 100 mg/ml streptomycin, and 1% L-glutamine at 37 °C in a 5% CO_2 atmosphere.

2.6 Cell viability assay

Cells were seeded into 96-well microtiter plates (BD Falcon, USA) at the density of 30×10^3 cells/well and allowed to attach for 24 h. After incubation, the medium was removed and a fresh cell growth medium was added (100 μl/well).

Diatomite nanoparticles at concentrations of 0, 20, 50, 100, 200, and 300 μg/ml were added into different wells in triplicate and incubated with cells for 24, 48, and 72 h. After treatment, the cell viability was assessed using MTT assay. 10 μl of a 5 mg/ml MTT solution in RPMI 1640 no phenol red (Sigma) was added to each well. Plates were then incubated under cell culture conditions for 3 h. Subsequently, 100 μl of MTT solvent (HCl 0.1 N in isopropanol) was added to each well and incubated for 1 h at room temperature with stirring to dissolve the formazan crystals. Absorbance of each sample was detected by Microplate Reader 680 (Biorad) at 570 nm.

2.7 Diatomite chemical functionalization

After purification treatments, diatomite surface was amino-modified by incubation with a 5% (v/v) (3-Aminopropyl)triethoxysilane (APTES) solution in absolute ethanol, following typical silanization processes [38,39]. Briefly, the reaction was performed for 1 h at room temperature with stirring in dark condition. Dispersion was then

centrifuged for 30 min at 15,000 ×g and supernatant was removed. The functionalized diatomite was washed twice with absolute ethanol; the collected pellet was incubated for 10 min at 100 °C (curing process). After incubation, the sample was resuspended and washed twice with absolute ethanol and then twice with PBS 1× pH 7.4.

2.8 Fourier-transform infrared spectroscopy

Chemical composition of APTES-functionalized diatomite nanoparticles was analyzed by Fourier-transform infrared (FTIR) spectroscopy. Spectra were recorded by a Thermo-Nicholet NEXUS Continuum XL (Thermo Scientific, Waltham, MA, USA) equipped with a micro- scope, at 2 cm^{-1} resolution on samples deposited on silicon chips (p-type, 0.003 ohm cm resistivity, <100 > oriented, 500-μm tick) of about 1 cm × 1 cm.

2.9 Nanopowder diatomite labeling

Diatomite labeling procedure was based on the use of an aminoreactive molecule, tetramethylrhodamine isothiocyanate. TRITC powder was solved in dimethyl sulfoxide (DMSO) and incubated with diatomite nanopowder in the presence of NaHCO$_3$ 0.1 M pH 8.7 with stirring for 1 h at room temperature in dark conditions. Subsequently, the sample was washed with distilled water to remove TRITC excess, until no fluorescence was revealed in the supernatant when analyzed by fluorescence microscopy. Labeled diatomite nanoparticles will be indicated as DNPs*.

2.10 Confocal microscopy

H1355 cell line (20×10^3 cells/coverslip) was plated on 10-mm glass coverslips placed on the bottom of 24-well plate, allowed to attach for 24 h under normal cell culture conditions, and then incubated with increasing DNPs* concentration (5, 10, 15 μg/mL) for 24 h. As negative control, the last supernatant obtained from nanoparticles labeling procedure was added to the cells. Cell nuclei and membranes

were then stained with Hoechst 33342 (Invitrogen, Carlslab, CA, USA) and WGA-Alexa Fluor 488, respectively.

Images were acquired at 63× magnification on a LSM710 confocal fluorescence microscope (Carl Zeiss Inc., Peabody, MA, USA) with the appropriate filters.

2.11 Cross-linker chemistry

APTES-functionalized diatomite was incubated with 20 mM Sulfo-GMBS in PBS for 1 h with stirring at room temperature. Subsequently, the sample was washed twice with PBS 1× to remove Sulfo-GMBS excess.

2.12 Peptide/siRNA complex

The relative concentrations of peptide and siRNA required to form a stable complex have been investigated by incubating 50 pmol of siRNA with different amounts of arginine peptide for 2 h at room temperature in PBS, with a peptide/siRNA charge ratio ranging from 0 to 20.

The ratio between peptide (NH_3^+) and siRNA (PO_4^-) was defined as the nitrogen/phosphate (N/P) ratio. Peptide/siRNA complexes were analyzed by electrophoretic mobility shift assay (EMSA) on a 20% polyacrylamide gel in TAE (40 mM Tris acetate/2 mM EDTA) buffer at 100 V for 70 min, followed by staining with ethidium bromide (EtBr) for 20 min.

In addition, the stability of siRNA to nuclease was evaluated in the absence and presence of poly-Arg peptide. The samples were incubated in PBS for 30 min in the presence of human pancreatic ribonuclease, gently provided by Prof. De Lorenzo, that is able to degrade double-strand RNA [40]. Samples were then analyzed by EMSA.

Finally, in order to assess the optimal peptide concentration, Sulfo-GMBS modified diatomite was incubated with increasing concentra-

tions (75, 150, 300 µM) of labeled peptide and fluorescence intensity was analyzed.

2.13 siRNA loading
0.5 mg of sulfo-GMBS modified diatomite was incubated with the complex formed by peptide and siRNA for 1 h at room temperature in dark condition.

Complex was obtained by mixing 150 µM peptide with 7.5 µM siRNA (molar ratio 20:1) in the presence of a 10-fold molar excess with respect to the peptide concentration of a reducing agent, Tris(2-carboxyethyl)phosphine hydrochloride (TCEP), in 1× PBS at room temperature for 2 h in dark condition [41,42]. Subsequently, diatomite suspension was centrifuged and the pellet was collected and washed twice with PBS 1×.

The siRNA loaded was about 0.7 pmol per 1.0 µg of diatomite, as determined by UV reading at 260 nm.

2.14 Fluorescence microscopy
Fluorescence of diatomite modified with Dy547 labeled siRNA (siRNA*) was investigated by means of Leica Z16 APO fluorescence macroscope equipped with a camera Leica DFC300, using an optics constituted by a 515–560 nm band-pass excitation filter, a 580 nm dichromatic mirror, and a 590 nm suppression filter. Analysis was performed on diatomite samples deposited on silicon substrates. Fluorescence values reported in the work are the average of three different measurements.

2.15 siRNA release profile
The siRNA release profile was performed by suspending siRNA* modified diatomite in 20 mM TrisHCl pH 7.5 and 20 mM NaCl at room temperature and then monitoring the fluorescence intensity in the supernatant and in diatomite at different time points. Images were

acquired on an Axiovert 40 CFL Zeiss and fluorescence intensity was analyzed by using ImageJ software 1.41o (http://imagej.nih.gov/ij/).

2.16 Confocal microscopy of nanoparticles internalization

Cells (50 × 10^3/coverslip) were plated on 10 mm glass coverslips placed on the bottom of 24-well plate, allowed to attach for 24 h under normal cell culture conditions and then incubated with siRNA* modified diatomite nanoparticles (300 μg/ml) for 18 h. Cells were washed with PBS, fixed in 4% formaldehyde for 30 min, washed 3 times with PBS and stained with membrane stain WGA-Alexa Fluor 488 Conjugate (Invitrogen, Carlslab, CA) according to the manufacturer's instructions. Cell nuclei were then stained with Hoechst 33342 (Invitrogen, Carlslab, CA).

Images were acquired at 63× magnification on a LSM710 confocal fluorescence microscope (Carl Zeiss Inc., Peabody, MA) with the appropriate filters.

2.17 Gene knockdown

Cells (150 × 10^3/well) were seeded into six-well plates 24 h before incubation with GAPDH and non-targeting (SCR) siRNA modified diatomite nanoparticles (100 pmol siRNA/140 μg diatomite) in RPMI1640. After 72 h of incubation, the cells were used for Western blot analysis.

Transfection with 100 pmol GAPDH and SCR siRNAs by using Lipofectamine 2000 (LF2000) according to the manufacturer's instructions (Invitrogen) was used as comparison.

H1355 cells were scraped, washed twice in cold 1× PBS, and resuspended in 20–40 μl of lysis buffer (50 mM Tris HCl pH 7.4, 1% NP40, 0.25% sodium deoxycholate, 150 mM NaCl, 1 mg/ml aprotinin, leupeptin, pepstatin, 1 mM Na_3VO_4, 1 mM NaF) for 30 min on ice and centrifuged at 14,000 ×g for 20 min at 4 °C.

Protein concentration was determined by a modified Bradford method, using the Bio-Rad protein assay and compared with BSA

standard curve. Cytosolic proteins (10 µg) were separated by SDS-PAGE, electrotransferred to nitrocellulose and reacted with the different antibodies. Blots were then developed using enhanced chemiluminescence detection reagents (SuperSignal West Pico, Pierce) and exposed to X-ray film. All films were scanned for densitometric analysis by using ImageJ 1.41o software (http://imagej.nih.gov/ij/).

3. Results

3.1 Characterization of diatomite nanoparticles

Natural diatomite are generally contaminated by organic residues and inorganic oxides [17,19]. Biomedical applications require strong purification treatments of vectors in order to obtain pure silica as safe and biocompatible material. Fig. 2 shows SEM images of diatomite deposited on silicon support, before (A) and after (B) purification treatments in strong hot acids.
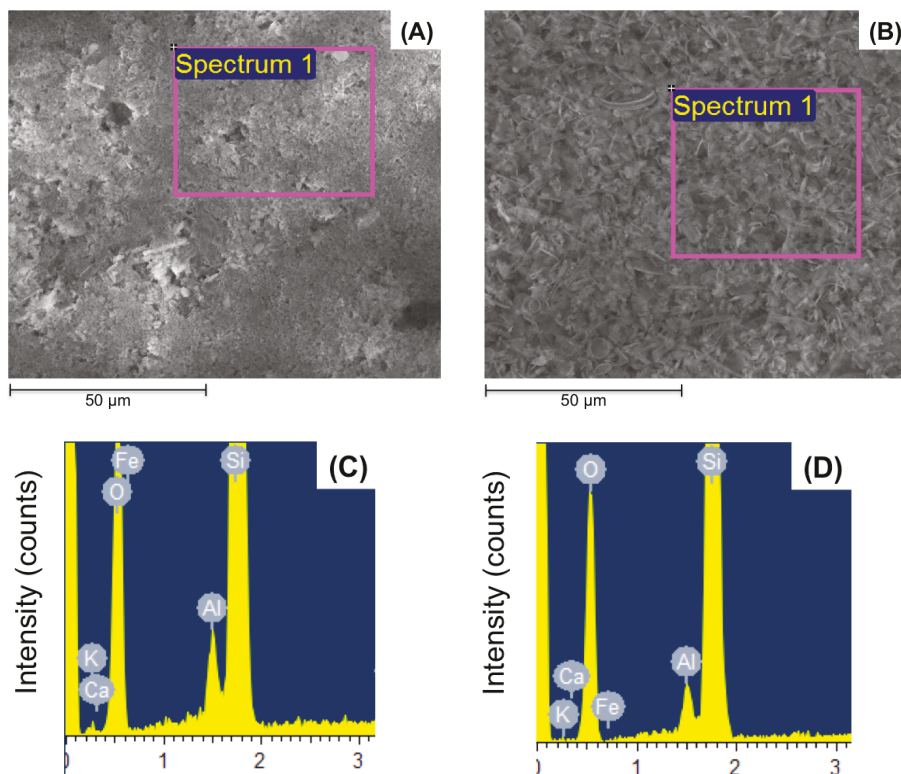
Figure 2 SEM images of diatomite deposited on silicon before (A) and after (B) purification treatments; corresponding EDS graphs (C–D).

14

Before purifications, the features of diatomite were completely masked by the presence of many impurities on their surface; EDS spectra showed changes in chemical composition of the samples: after cleaning treatments, the intensities of peaks corresponding to calcium, iron and aluminum decreased, whereas the silica peak increased (Fig. 2C and D). Detailed chemical composition of diatomite before and after purification is summarized in Table 1.

Table 1 Chemical composition of frustules before and after purification treatments.

Compounds	Before purification treatment (%)	After purification treatment (%)
SiO_2	92.1	94.6
Al_2O_3	3.3	2.7
K_2O	1.0	0.8
CaO	1.8	0.9
Fe_2O_3	1.8	1.0

The purification procedures have also been investigated by photoluminescence analysis.

Under UV excitation (325 nm), diatomite samples showed a blue photoluminescence, clearly visible by naked eye. Even if the origin of this emission is not completely clear, it is commonly believed that it is mainly originated from surface defects including OH^- groups and oxygen vacancies [43]. Laser pumping generates excited electrons whose radiative decay produces photoluminescence emission.

Fig. 3 shows the comparison between photoluminescence spectra of diatomite before (A) and after (B) treatments. The untreated sample was characterized by a weak signal with three main features peaked at 390 nm (3.18 eV), 460 nm (2.7 eV), and 500 nm (2.48 eV).

After treatment, the peak at 390 nm became weaker, another peak at 423 nm (2.93 eV) appeared, while the feature at 500 nm shifted to 490 nm (2.53 eV). These modifications were due to the removal of metallic impurities from the diatomite surface. The absence of impurities significantly modified the photoluminescence signal

changing reactions of energy transfer by surface radiative recombination.
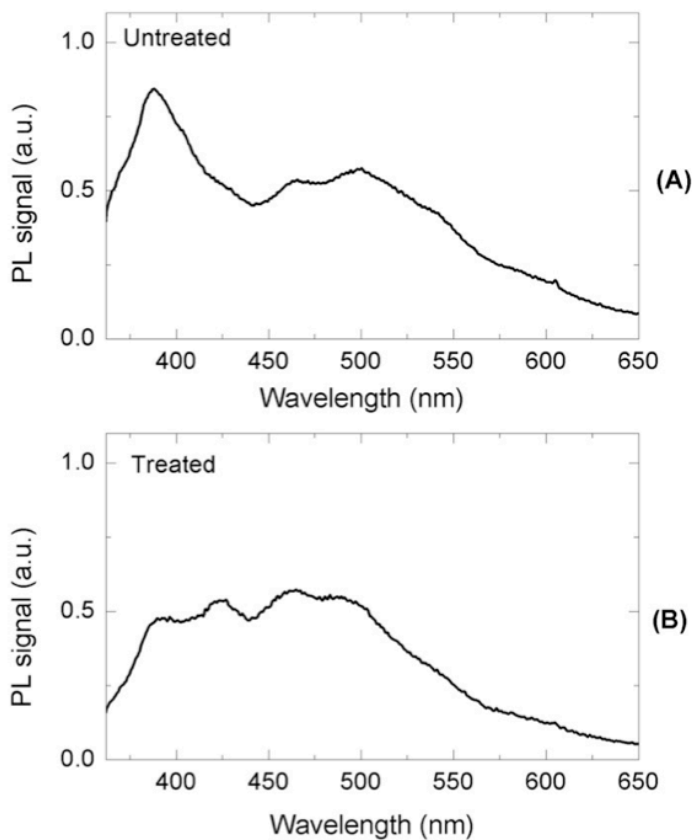
Figure 3 Photoluminescence spectra of untreated diatomite (A) and diatomite after piranha and HCl treatments (B).

Size and surface charge of purified diatomite nanoparticles dispersed in water (pH = 7) were determined by DLS. The average size and zeta-potential of nanoparticles were 220 ± 90 nm and -19 ± 5 mV,

respectively (Figure 4). The negative value of zeta-potential was due to the presence of silanol groups on nanoparticles surface after treatment in Piranha solution.
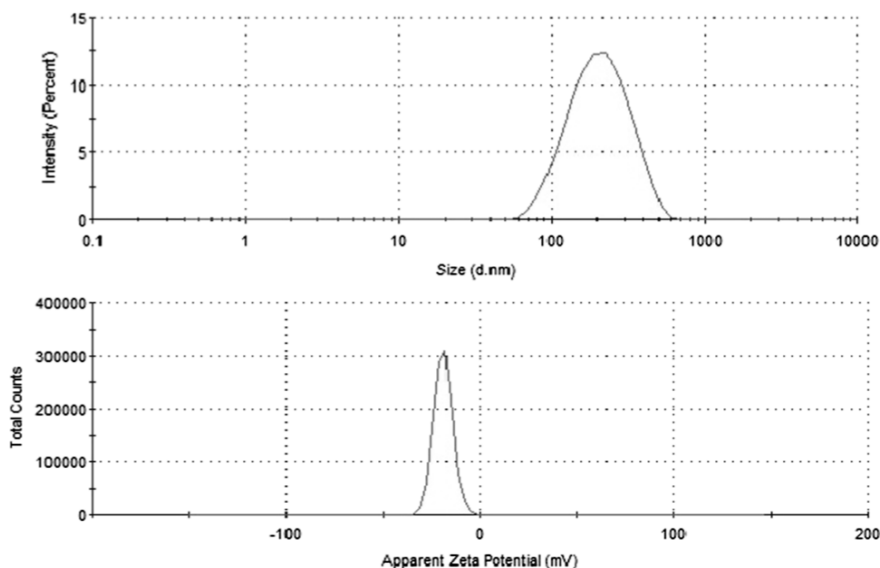
Figure 4 Size (upper graph) and zeta potential (lower graph) distributions of diatomite nanoparticles in water (pH = 7)

3.2 Biocompatibility

A critical issue for biomedical applications of new nanocarriers for drug delivery is the evaluation of their potential toxicity and biocompatibility [30,36,37].

In vitro cytotoxicity of DNPs was evaluated by MTT assay, a method based on the reduction of 3-(4,5-dimethythiazol- 2-yl)-2,5-diphenyl tetrazolium bromide by cellular oxidoreductases of viable cells, that yield a crystalline blue formazan product. H1355 cells were incubated with different concentrations of diatomite nanoparticles for 24, 48 and 72 h. The results obtained are reported in Fig. 5.

The exposure of H1355 cells to increasing nanoparticle concentrations (20 μg/ml, 100 μg/ml, 200 μg/ml and 300 μg/ml) induced very low toxicity being the average viability of the cells slightly lower than 100%. This result also demonstrated that the irregular shape of diatomite nanoparticles did not influence cell growth and morphology. In conclusion, the MTT assay showed that H1355 cell viability was not affected even after 72 h of exposure to diatomite nanopowder concentration up to 300 μg/ml, thus confirming their usability as nanovectors in nanomedicine for therapeutic applications [44,45].
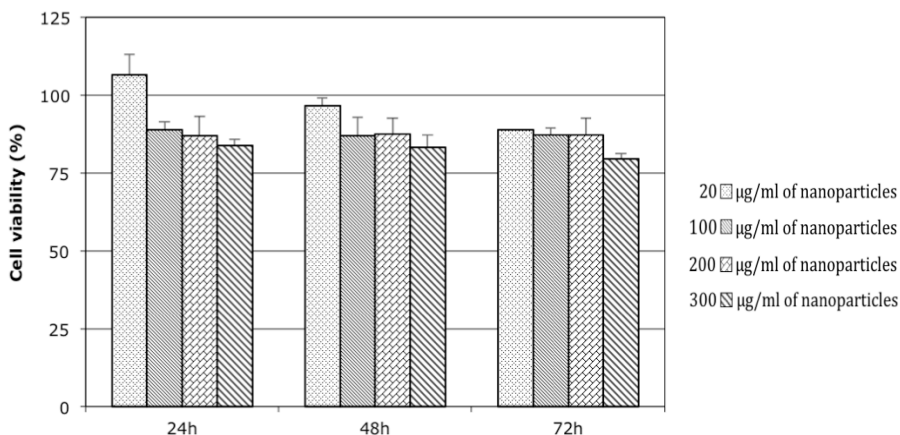
Figure 5 Cytotoxicity assessment of diatomite nanoparticles using MTT assay. Cell viability of H1355 cells treated with 20, 100, 200 and 300 µg/ml of nanoparticles for 24, 48 and 72 h at 37 °C. Data represent the mean ± s.d. (n = 3). Cell viability was expressed as the percentage of viable cells compared with cells cultured without nanoparticles as control (100%).

3.3 Silanization

Hot acid-treated nanoparticles were functionalized with APTES solution to allow an aminosilane coating on their surface. The functionalization procedure is fully sketched in scheme 1.
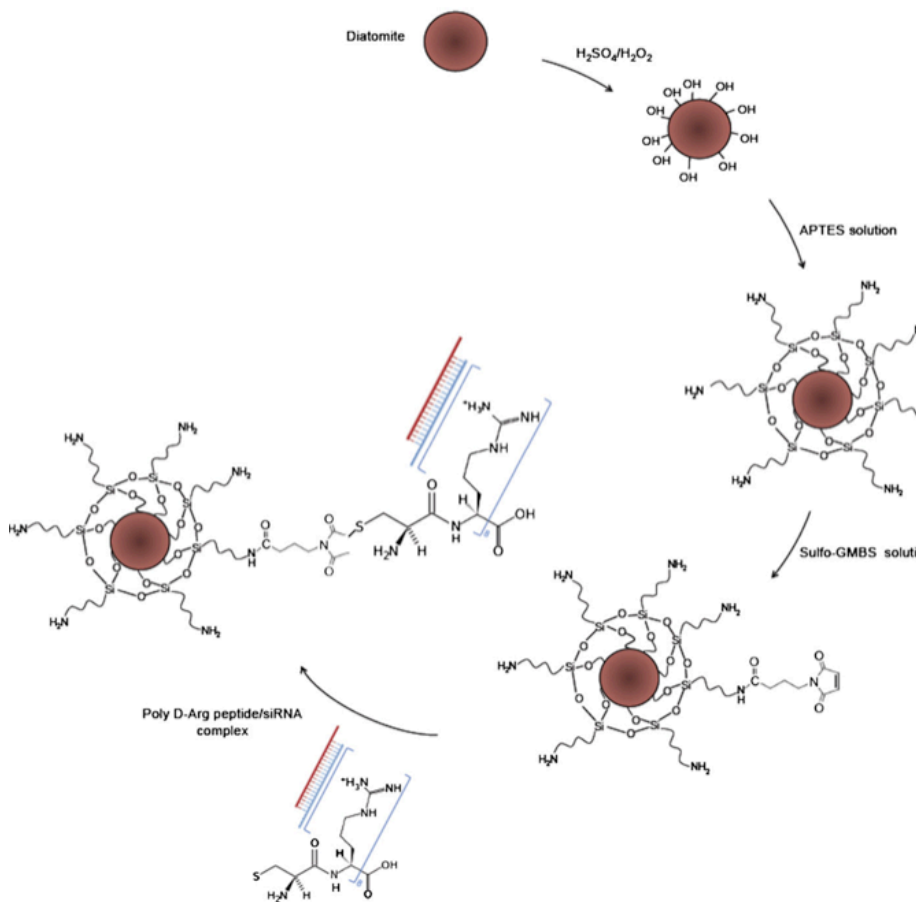
Scheme 1 Simplified functionalization scheme of diatomite nanoparticles with labeled siRNA (siRNA*).

Silanol groups on diatomite surface were formed by hydroxylation using aqueous sulfuric acid. APTES in organic anhydrous solvent reacted with silanol groups on the activated surface producing siloxane linkages.

Diatomite silanization was evaluated by FTIR spectroscopy. The

comparison between FTIR spectra of bare nanoparticles (upper graph) and APTES-functionalized powders (lower graph) is reported in Figure 6. The peak of Si-O-Si bond at 1,100 cm^{-1}, characteristic of diatomite frustules, is well evident in both spectra. Before APTES functionalization, it is also detected the peak at 3,700 to 3,200 cm^{-1} corresponding to Si-OH group. The spectrum of functionalized sample showed the silane characteristic peaks in the range between 1,800 and 1,300 cm^{-1} (see the inset of Figure 4); in particular, the peak at 1,655, corresponding to imine group and the peak at 1,440 cm^{-1}, corresponding to asymmetric deformation mode of the CH$_3$ group, were observed, according to results already reported [46,47]. FTIR characterization clearly demonstrated the silanization of silica nanoparticles.
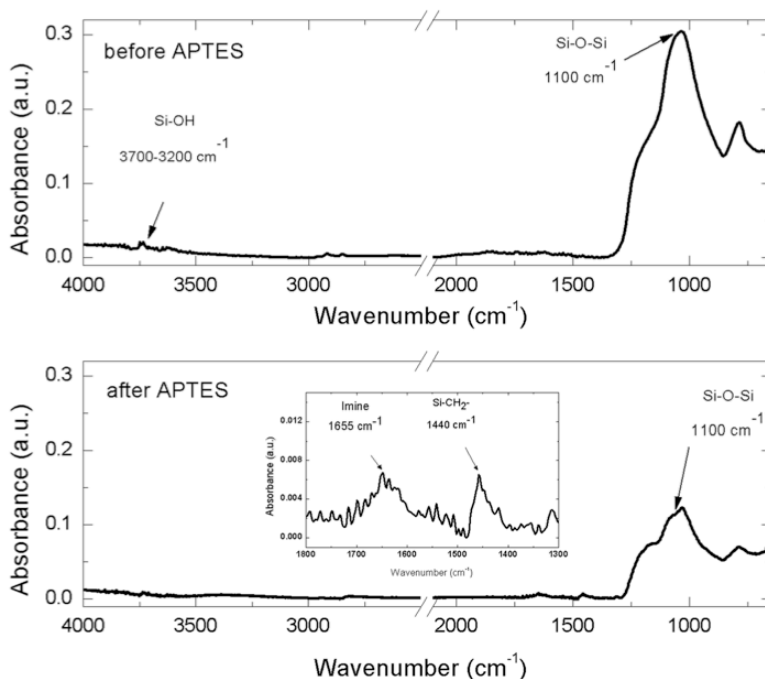
Figure 6 FTIR spectra of nanoparticles before (upper graph) and after (lower graph) APTES functionalization

3.4 Confocal microscopy analysis and DNPs* internalization

Nanoparticle cell uptake was studied by using DNPs* and confocal microscopy analysis. H1355 cells have been incubated with DNPs* at increasing concentrations (5, 10, 15 μg/mL) for 24 h. Figure 7 shows representative confocal microscopy images of cells treated with DNPs* compared to untreated cells as control. Cell nuclei were stained with Hoechst 33342 (blue), cell membranes were stained with WGA-Alexa Fluor 488 (green), and DNPs were labeled with TRITC (red). Images show an increase of fluorescence intensity at increasing DNPs* concentration and a homogeneous particles distribution in the cytoplasm and into nuclei.
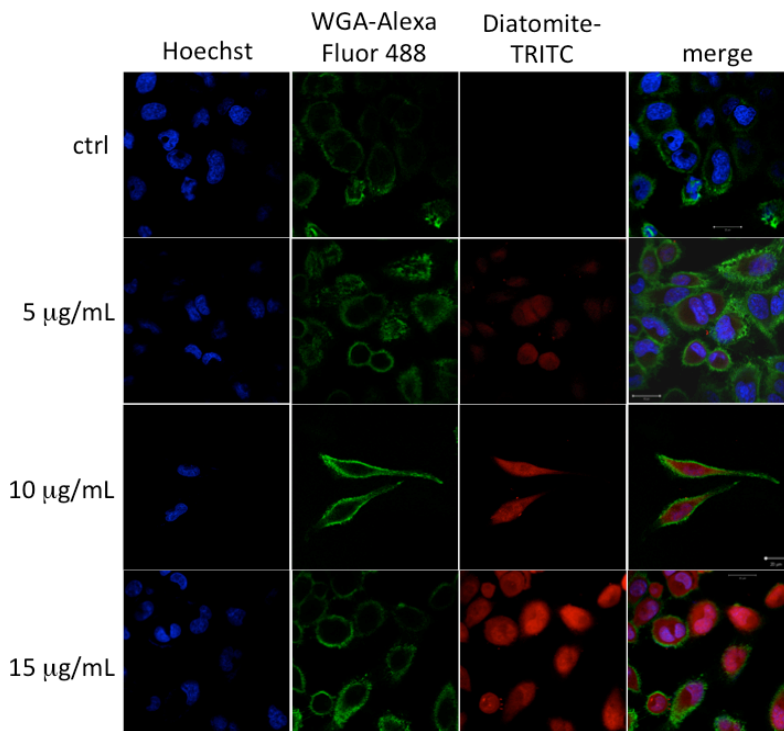
Figure 7 Confocal microscopy image of H1355 cells incubated with different concentrations of DNPs*; scale bar corresponds to 20 μm.

21

To prove the internalization of the carriers in the cells, images at different focal depth were recorded. Figure 8 shows that going from upper cell surface to the focus inside the cells, an increase of red diatomite fluorescence can be observed thus indicating the uptake of DNPs* by H1355 cells.
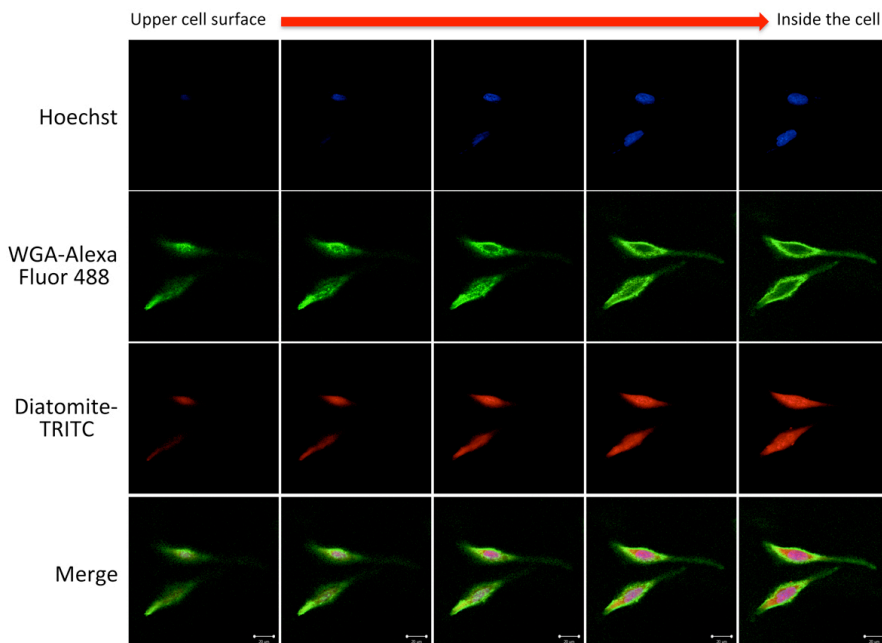
Figure 8 Confocal microscopy image with different focal depth of H1355 cells incubated with 10 μg/mL of DNPs*.

3.5 Study of siRNA loading into diatomite nanoparticles and in vitro release

siRNA*, complexed with a poly D-Arg peptide, was loaded onto diatomite nanoparticles following the functionalization procedure sketched in Scheme 1. Briefly, APTES-functionalized diatomite reacts with sulfo-GMBS, a heterobifunctional cross linker reactive to amino groups at one end and to sulfhydryl groups at the other. The NHS

ester reacts with the amino-modified diatomite surface as a nucleophile with release of the sulfo-NHS leaving group forming an amide bond. Peptide/siRNA* complex (molar ratio 20:1) was immobilized on the diatomite surface through the thioether bond between the sulfhydryl group of peptide cysteine residue and C-C bond of the maleimide ring of Sulfo-GMBS. A nonpolar homopeptide was used as control for aspecific interactions with siRNA.

The molar ratio peptide/siRNA* used in the functionalization proce-dure has been established by a gel shift assay, highlighting the complex electrostatic interaction as function of the positive peptide (NH_3^+)/negative RNA (PO_4^-) charge ratios. siRNA (50 pmol) was mixed with arginine peptides at various N/P ratios (0–20). The results showed that the electrophoretic migration of RNA was retarded with an increasing ratio of peptide/RNA (Fig. 9A).
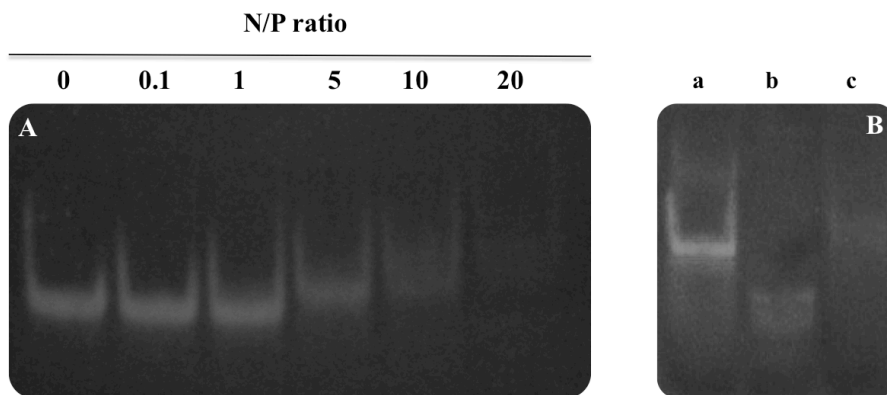
Figure 9 (A) Poly D-Arg peptide (N) and siRNA (P) were incubated at different molar ratios (range 0–20, as indicated above each lane) and the formed complex was analyzed by gel shift. (B) Effect of HP-RNase on siRNA degradation; siRNA alone (lane a), siRNA incubated with HP-RNase in absence (lane b) or in the presence (lane c) of poly D-Arg peptide.

The intensity of the siRNA band decreased as the N/P ratio increased. No siRNA band was observed at the N/P ratio of 20. This absence of migration was probably due to the complete neutralization of nucleic

acid charge by the arginine peptide and/or formation of a large complex between the arginine and siRNA. These results strongly suggest that an arginine peptide made of 8 residues could be sufficient to form a complex with a siRNA.

In addition, since the first biological barrier of siRNA delivery is its susceptibility to nucleases that causes its rapid degradation, the capability of the peptide/siRNA complex to protect siRNA from nuclease degradation was investigated. For this purpose, human pancreatic ribonuclease (HP-RNase), able to degrade double-strand RNA, was used [40]. As shown in Fig. 9B, siRNA was rapidly degraded by HP-RNase (lane b), while, when preincubated with peptide before adding RNase, no significant degradation was observed (lane c). Our data confirmed that a poly D-Arg peptide strongly interacts with siRNA forming a highly stable complex as previously reported [40,41]. Furthermore, the formation of the peptide/siRNA complex improved the siRNA stability protecting it from nuclease degradation [48].

Diatomite functionalization was evaluated by means of fluorescence microscopy and photoluminescence analysis.

The images reported in fig. 10A shows diatomite incubated with poly D-Arg peptide/ siRNA* (left image) and control peptide/siRNA* (right image). High red fluorescence (average intensity = 27 ± 2) was well evident only using poly D-Arg peptide/siRNA*; conversely, diatomite incubated with control peptide/siRNA* appeared darker (average intensity = 9 ± 1). The result was confirmed by PL measurements. PL spectra of diatomite functionalized with poly D-Arg peptide/siRNA* and control peptide/siRNA* are compared in Fig. 10B. Only the sample functionalized with specific peptide was characterized by a strong PL peak at 575 nm due to the presence of labeled nucleic acid.
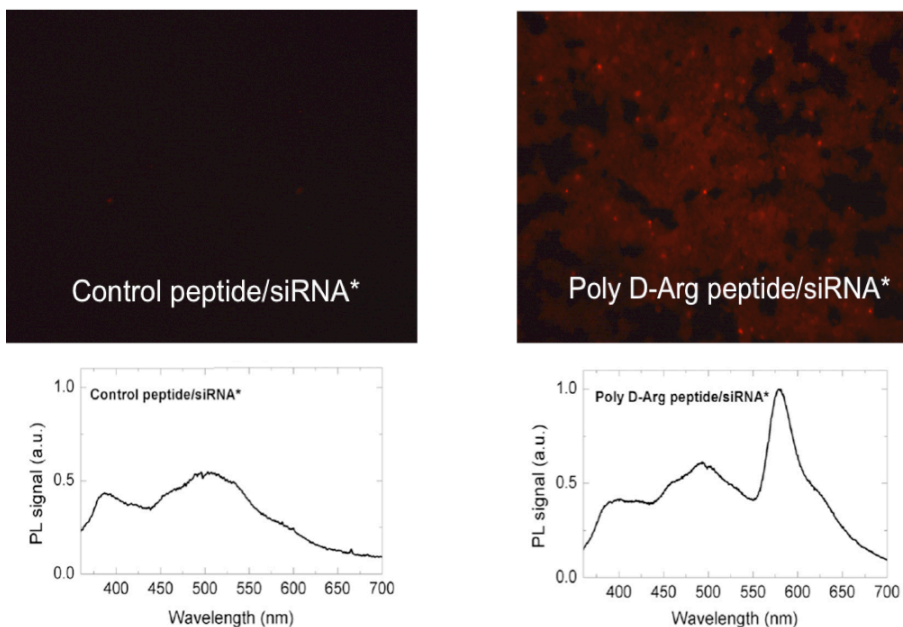
Figure 10 (A) Fluorescence microscopy images of diatomite modified with Poly D-Arg peptide/siRNA* (left image) and with a control peptide/siRNA* (right image); (B) corresponding photoluminescence spectra.

The capability of loaded diatomite to release in solution siRNA* was also investigated by measuring the fluorescence intensity of both supernatant and diatomite as function of time (Fig. 11). siRNA was released into supernatant in two phases: an initial phase of 12 h (burst release), followed by slow and sustained release phase over 48–72 h. The fluorescence profile of diatomite showed an opposite trend.

The slow siRNA release observed was probably due to the progressive weakening of the electrostatic interactions between peptide and nucleic acid.
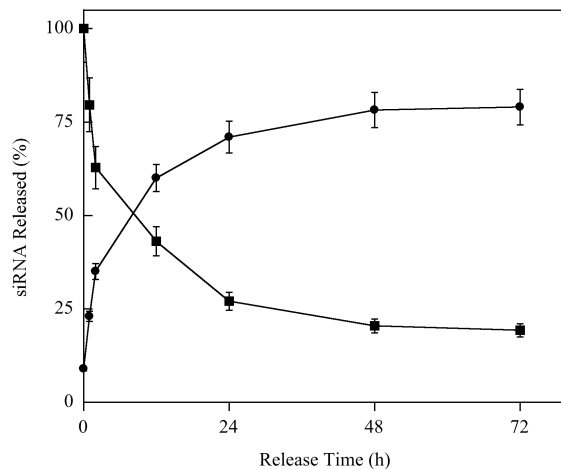
Figure 11 Fluorescent labeled siRNA bound to DNPs (DNPs–siRNA*) was incubated in 20 mM Tris–HCl and 20 mM NaCl, pH 7.5 at 37 °C and at time intervals the fluorescence intensity was measured in the sample supernatant (●) and diatomite (■).

H1355 cells were incubated with siRNA* modified diatomite nanoparticles (DNPs–siRNA*) to evaluate the siRNA uptake and cellular internalization. Fig. 12 shows a representative confocal microscopy image of cells treated with DNPs–siRNA* compared to untreated cells as control.

Fluorescence images show cell nuclei stained with Hoechst 33342 (blue) and cell membranes with WGA-Alexa Fluor 488 (green). Confocal microscopy analysis was performed after treatment with DNPs–siRNA* for 24 h.

In Fig. 12 the presence of siRNA (labeled with Dy547, red) into the H1355 cells treated with DNPs–siRNA* is evident. Merge image reveals that siRNA molecules are localized in the cytoplasm of cells and no signals were observed inside the nucleus. Red fluorescence (siRNA*) was found as both spots and diffuse signal [42,49-51].

The efficiency of DNPs–siRNA* internalization was quantified by fluorescence microscopy: counting the number of red fluorescent cells and the total number of cells (determined in bright field), a ratio of about 75% was calculated.
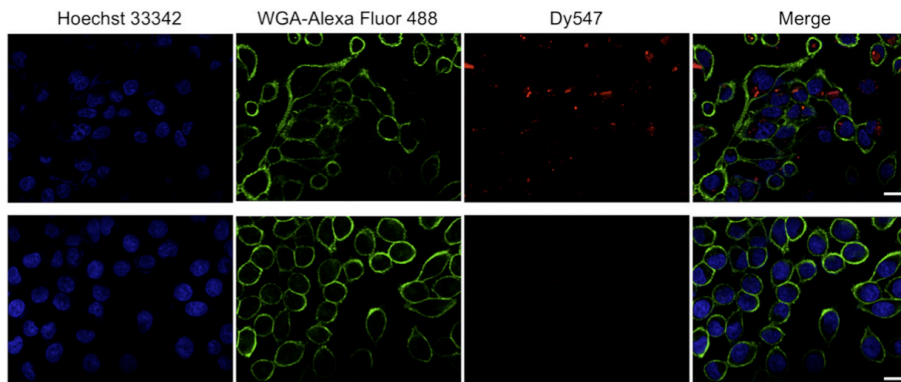
Figure 12 Confocal microscopy on cells treated with siRNA* modified diatomite nanovectors (first line) and untreated cells as control (second line). Cell nuclei and membranes were stained with Hoechst 33342 and WGA-Alexa Fluor 488, respectively. siRNA was labeled with Dy547. Scale bar corresponds to 20 μm.

3.6 Gene silencing

Finally, the ability of the DNPs–siRNA complexes to silence in H1355 cells targeted mRNA was investigated by Western blot analysis. In particular, a siRNA against glyceraldehyde 3-phosphate dehydrogenase (GAPDH) and a scramble siRNA as control were used. Moreover, to compare the efficiency of the DNPs–siRNA delivery system with that of other system, the commercially available Lipofectamine 2000 transfection reagent was used. The obtained results are reported in Fig. 13.
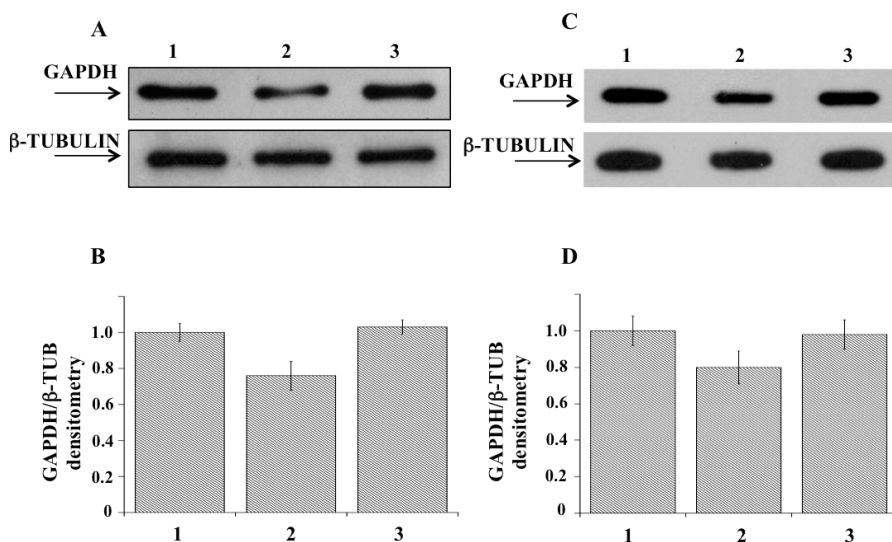
Figure 13 (A) Immunoblotting analysis of GAPDH (upper gel) and of β-tubulin (lower gel) of protein expression in DNPs–siRNA treated cells. Lanes: 1) control cells; 2) DNPs–GAPDH–siRNA; 3) DNPs–SCR–siRNA. (B) Densitometric intensity band ratio of GAPDH and β-tubulin used as internal control. The intensities of the bands were expressed in arbitrary units. (C) Immunoblotting analysis of GAPDH (upper gel) and of β-tubulin (lower gel) protein expression in lipofectamine-siRNA transfected cells. Lanes: 1) control cells; 2) GAPDH–siRNA; and 3) SCR–siRNA. (D) Densitometric intensity band ratio of GAPDH and β-tubulin used as internal control. The intensities of bands were expressed in arbitrary units. Each measurement and Western blot was carried out in triplicate. Error bars indicate the maximum deviation from the mean value of two independent experiments

Compared to untreated cells, GAPDH protein expression level after incubation of the cells with DNPs–siRNA complexes at 37 °C for 48 h was reduced (Panel A, upper gel) of about 22% (lane 2) as evaluated from the densitometric intensity of the bands (Panel B). Cells incubated with DNPs–SCR–siRNA (lane 3) showed instead almost identical protein expression level as control (lane 1), thus

28

demonstrating the selective inhibition by siRNA. Panels C and D report the expression level and the densitometric analysis, respectively, of cells transfected with lipofectamine. In this case, GAPDH protein expression level (lane 2) was down-regulated of about 20%.

Even if the delivery efficiency of DNPs and lipofectamine 2000 is similar, the use of diatomite as nanocarrier is more suitable for medical applications since it allows: slow release of the loaded drug, loading with one or more different molecules (e.g. siRNA + drug), biocompatibility and selective targeted functionalization to improve the delivery of anti-tumoral molecules to specific cell population.

4. Conclusions

Nanocarriers have emerged as an important tool for clinical applications and tumor-specific delivery of siRNA has great potential for successful targeted cancer therapy. In this work, a procedure to make diatomite, a natural porous biomaterial of sedimentary origin, suitable for the delivery of anticancer molecules into cells was settled. Purified diatomite nanoparticles morphology and surface chemical modifications were investigated by scanning electron microscopy equipped by energy dispersive X-ray spectroscopy, photoluminescence, dynamic light scattering measurements and Fourier transform IR spectroscopy. *In-vitro* toxicity studies highlighted the non-toxic nature of nanoparticles. An effective uptake of the engineered nanovectors into human epidermoid carcinoma cells, localized both in cytoplasm and nucleous, was observed after functionalization with APTES and labeling with tetra-methylrhodamine isothiocyanate. Subsequently, when a labeled small interfering RNA was loaded on the nanoparticles, confocal microscopy analysis revealed an efficient nanoparticle uptake exclusively into cytoplasm. Finally, NPs loaded with siRNA were able to induce gene silencing at a level comparable with that of common transfectans.

These findings demonstrate that diatomite nanoparticles, with their versatile structure and porosity, could represent a promising tool for the delivery of anticancer molecules such as siRNA, probably miRNA and drugs, inside cancer cells. Nevertheless, to create DNPs suitable for clinical applications, without undesirable side effects, better and more extensive *in vivo* testing is required.

Moreover, it would be expected that compared to other nanocarriers, their selective targeted functionalization will improve the delivery of anti-tumoral molecules to specific cell population.

5. References

1) Orive, G., Hernandez, R.M., Rodriguez Gascon, A., Dominguez-Gil, A., Pedraz, J.L. (2003). Drug delivery in biotechnology: present and future. Curr. Opin. Biotechnol. 14, 659-664.

2) Langer, R. (1990). New methods of drug delivery. Science 249, 1527-1533.

3) Juliano, R.L. (1978). Drug delivery systems: a brief review. Can. J. Physiol. Pharmacol . 56, 683-90.

4) Parveen, S., Sahoo, S.K. (2006). Nanomedicine: clinical applications of polyethylene glycol conjugated proteins and drugs. Clin. Pharmacokinet. 45, 965-88.

5) Lee, H.J. (2002). Protein drug oral delivery: the recent progress. Arch. Pharm. Res. 25, 572-84.

6) Kayser, O., Lemke, A., Hernandez-Trejo, N. (2005). The impact of nanobiotechnology on the development of new drug delivery systems. Curr. Pharm. Biotechnol. 6, 3-5.

7) Parveen, S., Misra, R., Sahoo, S. K. (2012). Nanoparticles: a boon to drug delivery, therapeutics, diagnostics and imaging. Nanomedicine: Nanotechnology, Biology, and Medicine. 8, 147-166

8) Goldberg, M., Langer, R., and Jia, X. (2007). Nanostructured materials for applications in drug delivery and tissue engineering. J. Biomater. Sci. Polym. 18, 241-246

9) Mok, H., Bae, K.H., Ahn, C.H., and Park, T.G. (2009). PEGylated and MMP-2 specifically dePEGylated quantum dots: comparative evaluation of cellular uptake. Langmuir 25, 1645-1650.

10) Peer, D., Karp, J.M., Hong, S., Farokhzad, O.C., Margalit, R., and Langer, R. (2007). Nanocarriers as an emerging platform for cancer therapy. Nat. Nanotechnol. 2, 751-760.

11) Potter, R.F., and Groom, A.C. (1983). Capillary diameter and geometry in cardiac and skeletal muscle studied by means of corrosion casts. Microvasc. Res. 25, 68-84.

12) Bartlett, D.W., and Davis, M.E. (2007). Physicochemical and biological characterization of targeted, nucleic acid-containing nanoparticles. Bioconjugate Chem. 18, 456-468.

13) Lee, H., Lee, K., and Park, T.G. (2008). Hyaluronic acid-paclitaxel conjugate micelles: synthesis, characterization, and antitumor activity. Bioconjugate Chem. 19, 1319-1325.

14) Hong, S., Leroueil, P.R., Majoros, I.J., Orr, B.G., Baker, J.R. Jr, and Banaszak Holl, M.M. (2007). The binding avidity of a nanoparticle based multivalent targeted drug delivery platform. Chem. Biol. 14, 107-115.

15) Montet, X., Funovics, M., Montet-Abou, K., Weissleder, R., and Josephson, L. (2006). Multivalent effects of RGD peptides obtained by nanoparticle display. J. Med. Chem. 49, 6087-6093.

16) Marianecci, C., Di Marzio, L., Rinaldi, F., Celia, C., Paolino, D., Alhaique, F., Esposito, S., Carafa, M. (2014). Niosomes from 80s to present: the state of the art. Adv. Colloid Interface Sci. 205, 187-206.

17) Şan, O., Gören, R., Özgür, C. (2009). Purification of diatomite powder by acid leaching for use in fabrication of porous ceramics. Int. J. Miner. Process. 93, 6-10.

18) Wang, Y., Cai, J., Jiang, Y., Jiang, X., Zhang, D. (2013). Preparation of biosilica structures from frustules of diatoms and

their applications: current state and perspectives. Appl. Microbiol. Biotechnol. 97, 453-462.

19) Goren, R., Baykara, T., Marsoglu, M. (2002). A study on the purification of diatomite in hydrochloric acid. Scand. J. Metall. 31, 115-119.

20) Goren, R., Baykare, T., Marsoglu, M. (2002). Effects of purification and heat treatment on pore structure and composition of diatomite. Br. Ceram. Trans. 101, 177.

21) Xiaohua, Q., Mingzhu, L., Zhenbin, C., Rui, L. (2007). Preparation and properties of diatomite composite superabsorbent. Polym. Adv. Technol. 18, 184-193.

22) Bens, E.M., Drew, C.M. (1967). Diatomaceous earth: scanning electron microscopy of Chromosorb P. Nature. 216, 1046.

23) Carter, M.J., Milton, I.D. (1993). An inexpensive and simple method for DNA purifications on silica particles, Nucleic Acids Res. 21, 1044.

24) Khraisheh, M.A.M., Al-Ghouti, M.A., Allen, S.J., Ahmad, M.N. (2005). Effect of OH and silanol groups in the removal of dyes from aqueous solution using diatomite. Water Res. 39, 922-932.

25) Parker, A.R., Townley, H.E. (2007). Biomimetics of photonic nanostructures, Nat. Nanotechnol. 2, 347-353.

26) Xu, F., Wang, Y., Wang, X., Tang, Y., Yang, P. (2003). A novel hierarchical nanozeolite composite as sorbent from protein separation in immobilized metal-ion affinity chromatography. Adv. Mater. 15, 1751-1753.

27) Kim, J., Seidler, P., Wan, L.S., Fill, C. (2009). Formation, structure, and reactivity of amino- terminated organic films on silicon substrates. J. Colloid Interface Sci. 329, 114-119.

28) De Stefano, L., Lamberti, A., Rotiroti, L., De Stefano, M. (2008). Interfacing the nanostructured biosilica microshells of the marine diatom Coscinodiscus wailesii with biological matter. Acta Biomater. 4, 126-130.

29) De Stefano, L., Rotiroti, L., De Stefano, M., Lamberti, A., Lettieri, S., Setaro, A., Maddalena, P. (2009). Marine diatoms as optical biosensors. Biosens. Bioelectron. 24, 1580-1584.

30) Zhang, H., Shahbazi, M.A., Mäkilä, E.M., da Silva, T.H., Reis, R.L., Salonen, J.J., Hirvonen, J.T., Santos, H.A. (2013). Diatom silica microparticles for sustained release and permeation enhancement following oral delivery of prednisone and mesalamine. Biomaterials. 34, 9210-9219.

31) Bariana, M., Aw, M.S., Kurkuri, M., Losic, D. (2013). Tuning drug loading and release properties of diatom silica microparticles by surface modifications. Int. J. Pharm. 443, 230-241.

32) Aagaard, L., Rossi, J.J. (2007). RNAi therapeutics: principles, prospects and challenges. Adv. Drug Deliv. 59, 75-86.

33) Gavrilov, K., Saltzman, V.M. (2012). Therapeutic siRNA: principles, challenges, and strategies. Yale J. Biol. Med. 85, 187-200.

34) Whitehead, K.A., Langer, R., Anderson, D.G. (2009). Knocking down barriers: advances in siRNA delivery. Nat. Rev. Drug Discov. 8, 129-138.

35) Mai, W.X., Meng, H. (2013). Mesoporous silica nanoparticles: a multifunctional nano therapeutic system, Integr. Biol. 5, 19-28.

36) Love, S.A., Maurer-Jones, M.A., Thompson, J.W., Lin, Y.S., Haynes, C.L. (2012). Assessing nanoparticle toxicity. Annu. Rev. Anal. Chem. 5, 181-205.

37) Lin, Y.S., Haynes, C.L. (2009). Synthesis and characterization of biocompatible and size-tunable multifunctional porous silica nanoparticles. Chem. Mater. 21, 3979-3986.

38) De Stefano, L., Oliviero, G., Amato, J., Borbone, N., Piccialli, G., Mayol, L., Rendina, I., Terracciano, M., Rea, I. (2013). Aminosilane functionalizations of mesoporous oxidized silicon for oligonucleotides synthesis and detection. J. R. Soc. Interface. 10, 20130160.

39) Terracciano, M., Rea, I., Politi, J., De Stefano, L. (2013). Optical characterization of aminosilane-modified silicon dioxide surface for biosensing. J. Eur. Opt. Soc. Rapid Publ. 8, 1303.

40) Sorrentino, S., Naddeo, M., Ruso, A., D'Alessio, G. (2003). Degradation of double-stranded RNA by human pancreatic ribonuclease: crucial role of noncatalytic basic amino acid residues. Biochemistry. 42, 10182-10190.

41) Kumar, P., Wu, H., McBride, J.L., Jung, K., Kim, M.H., Davidson, B.L., Lee, S.K., Shankar, P., Manjunath, N. (2007). Transvascular delivery of small interfering RNA to the central nervous system. Nature. 448, 39-43.

42) Simeoni, F., Morris, M.C., Heitz, F., Divita, G. (2003). Insight into the mechanism of the peptide-based gene delivery system MPG: implications for delivery of siRNA into mammalian cells. Nucleic Acids Res. 31, 2717-2724.

43) Setaro, A., Lettieri, S., Maddalena, P., De Stefano, L. (2007). Highly sensitive optochemical gas detection by luminescent marine diatoms. Appl. Phys. Lett. 91, 051921.

44) Serda, R.E., Gu, J., Bhavane, J.C., Liu, X.W., Chiappini, C., Decuzzi, P., Ferrari, M. (2009). The association of silicon microparticles with endothelial cells in drug delivery to the vasculature. Biomaterials. 30, 2440-2448.

45) Serda, R.E., Godin, B., Blanco, E., Chiappini, C., Ferrari, M. (2011). Multi-stage delivery nanoparticle systems for therapeutic applications. Biochim. Biophys. Acta. 1810, 317-329.

46) Kim, J., Seidler, P., Wan, L.S., Fill, C. (2009). Formation, structure, and reactivity of amino-terminated organic films on silicon substrates. J. Colloid Interface Sci. 329, 114-119.

47) Chiang, C.H., Ishida, H., Koenig, J.L. (1980). The structure of γ-aminopropyltriethoxysilane on glass surfaces. J. Colloid Interf. Sci. 2, 396.

48) Morris, M.C., Vidal, P., Chaloin, L., Heitz, F., Divita, G. (1997). A new peptide vector for efficient delivery of oligonucleotides into mammalian cells. Nucleic Acids Res. 25, 2730-2736.

49) Kim, S.W., Kim, N.Y., Choi, Y.B., Park, S.H., Yang, J.M., Shin, S. (2010). RNA interference in vitro and in vivo using an arginine peptide/siRNA complex system. J. Control. Release. 10, 335-343.

50) Nakamura, Y., Kogure, K., Futaki, S., Harashima, H. (2007). Octaarginine-modified multifunctional envelope-type nano device for siRNA. J. Control. Release. 119, 360-367.

51) Chen, A.M., Zhang, M., Wei, D., Stueber, D., Taratula, O., Minko, T., He, H. (2009). Co-delivery of doxorubicin and Bcl-2 siRNA by mesoporous silica nanoparticles enhances the efficacy of chemotherapy in multidrug-resistant cancer cells. Small. 5, 2673-2677